Mission Profile Based Reliability Analysis of A Bridgeless Boost PFC

Chen, Zhengge; Davari, Pooya; Wang, Huai

Published in:
2021 IEEE Applied Power Electronics Conference and Exposition, APEC 2021

DOI (link to publication from Publisher):
10.1109/APEC42165.2021.9487083

Publication date:
2021

Document Version
Early version, also known as pre-print

Mission Profile Based Reliability Analysis of A Bridgeless Boost PFC

Zhengge Chen[†,‡], Pooya Davari[†], *Senior Member*, *IEEE*, and Huai Wang[†], *Senior Member*, *IEEE*

[†]Center of Reliable Power Electronics
Department of Energy Technology
Aalborg University (AAU), Aalborg, Denmark
zgc@et.aau.dk, pda@et.aau.dk, hwa@et.aau.dk

[‡]Power Conversion and Control (PCC) Lab
School of Electrical Engineering
Southwest Jiaotong University (SWJTU), Chengdu, China
zgc@et.aau.dk / zhenggechen@163.com

***Abstract*—Bridgeless power factor correction (PFC) converters are gaining popularity in recent years mainly for the efficiency superiority over their conventional topology counterparts. However, the quantitative reliability analysis of the bridgeless topologies in the wear-out region is missing and their reliability performances compared with the conventional one are unknown. Thus, based on the telecom applications with a representative mission profile in a rural area, this paper employs a mission profile-based reliability analysis approach to estimate the failure probability of an input-parallel output-series (IPOS) bridgeless boost PFC converter, along with the conventional one. Based on the measured efficiency data obtained from the built prototypes, the reliability analysis results indicate that under the same design specifications and criteria, the accumulated failure of the IPOS bridgeless is 0.27% within 20 years of operation, much lower than that (2.06%) of the conventional boost PFC converter.**

***Index Terms*—Bridgeless, PFC, telecom, mission profile, reliability analysis, wear-out region.**

I. Introduction

THE bridgeless power factor correction (PFC) topologies have higher efficiency than their conventional topology counterparts due to the reduced conducting diodes in the diode bridges [1]. The recent decades have witnessed their growth in PFC applications with different types of bridgeless topologies proposed, compared, and optimized for performance improvements [1]–[4]. For example, the bridgeless boost type topology are evaluated and surveyed [1], different types of bridgeless family derivations and categories are given [2], zero-voltage switching of the totem-pole boost bridgeless for higher efficiency is proposed [3], novel bridgeless topology is proposed and optimized for electric vehicles [4].

However, among the aforementioned researches, bridgeless PFC converter-related quantitative reliability investigations are rarely seen [5]. In the real field, aluminum electrolytic capacitors (Al-Caps) are typically considered as one of the weak parts in terms of reliability. Thus, many PFC converter reliability-related researches [6] have mainly discussed how to eliminate the aluminum electrolytic capacitors (Al-Caps) for a long expected lifetime. Typical examples are the extensive studies of Al-cap-free LED drivers, which pursue the lifetime compatibility with the LED. Nevertheless, the key question that how much the lifespan improvement of the PFC converter without Al-Caps, is quantitatively not answered. On the other hand, many Al-Cap targeted reliability researches have been conducted [7]–[10], e.g., the Al-Cap lifetime prediction model for DC-DC converter [8], real-time Al-Cap condition monitoring and lifetime prediction method in uninterruptible power supplies [9], a physics-of-failure-based Al-Cap lifetime prediction method in LED drivers [10]. Unfortunately, among them, the detailed PFC converter level reliability research is not involved.

In fact, for power electronic products, including PFC converters, their reliability performance can be estimated quantitatively by empirical-based component reliability models [5], [11]–[14]. For example, the fixed failure rates of components extracted from U.S. Military-Handbook-217 are used to assess the lifetime of PFC converters [11], [12]. This reliability assessment approach is simple since only the constant failure rates of components are required. However, the disadvantage is low accuracy [15], because the constant failure rates are only the collected statistic data of random failures in useful life region [16]. Neither the component manufacturing differences, nor the product operation conditions (i.e., mission profiles) are considered. In contrast, Ref. [13] employs another statistic data-based reliability analysis method to investigate two different AC-DC topology configurations, which uses different fixed failure rates based on the manufacturers. Besides, Ref. [5] adopts the fixed failure rates provided by model IEC TR 62380 to evaluate the reliability performance of two different bridgeless boost PFC converters, which considers component manufacturing impacts.

Whereas, the fixed failure rate-based lifetime predictions do not consider the time-related device reliability behavior in the wear-out region [17]. Besides, they typically fail to reflect the reliability impacts of the mission profiles and control strategies, which can hardly be solved by the fixed failure rate numbers [14]. In order to overcome the above-mentioned barricades, this paper adopts a mission profile-based reliability analysis approach to evaluate the accumulated failure of the capacitors, MOSFETs, and diodes in the bridgeless and conventional boost topologies in the wear-out region.

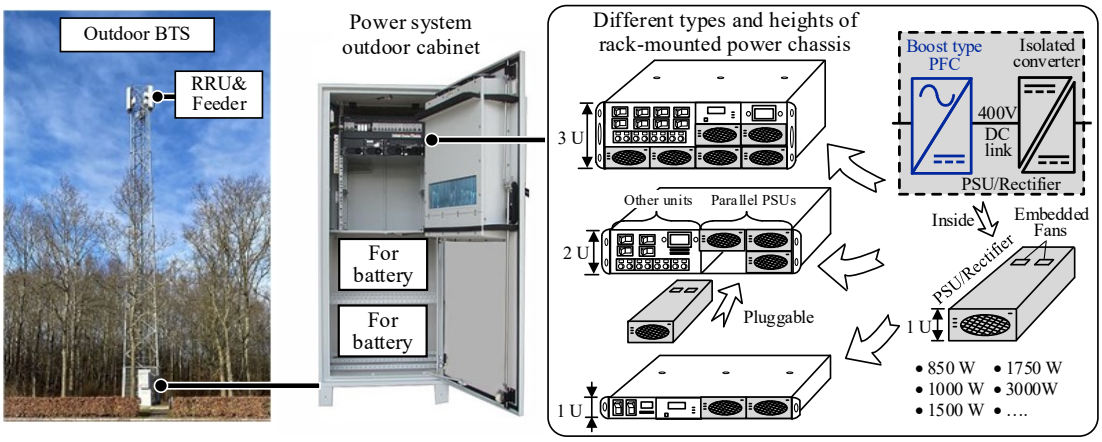

Fig. 1. Outdoor BTS application scenario of power supply unit (PSU)/rectifier with the boost type PFC in the different types of power chassis.

This approach is initially proposed in [18] to analyze DC-DC converter reliability for a backup power application and the specific load and ambient temperature mission profiles are considered to reflect the application impacts. Meanwhile, it has also been used to evaluate the reliability performance of a micro-inverter in photovoltaic (PV) applications [19] and modular multilevel converters (MMCs) [20].

Since the component wear-out failure is highly related to the thermal cycles, as the first step, the adopted reliability analysis approach essentially uses the mission profile data and converter-related parameters to estimate the component lifetime based on the calculated temperature cycles. Secondly, it generates probability-related results by means of several statistics-based models and Monte Carlo simulation. In fact, the first step of this reliability analysis approach is more important, related to the building of the electro-thermal loop and the use of mission profile data, which also makes the reliability analysis conducted in this paper different from what is presented in [18]–[20].

The rest of this paper is arranged as follows. In Section II, the mission profiles will be presented, along with the introduction of the studied bridgeless boost PFC converter. In Section III, the reliability analysis approach is presented with the estimated failure probability of the studied converters. The conclusion is drawn in Section IV.

II. Mission Profiles and Topology

The adopted reliability analysis approach has taken the mission profiles and the topologies into considerations. Thus, they have to be clarified firstly.

A. Applications and Mission Profiles

Fig. 1 shows the application scenario of the studied boost type PFC converters in the Telecom base transceiver station (BTS). It can be seen that there are different types of rack-mounted power chassis, which actually are selected mainly based on the load consumption as well as the business plans of the network operators. This paper mainly focuses on the BTS located in the rural area since their reliability issue is more concerned due to the inconvenient maintenance.

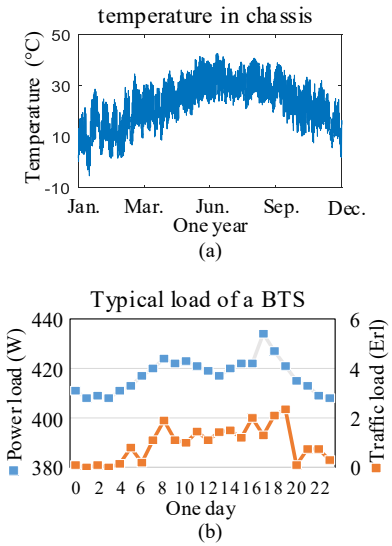

Fig. 2. Considered rural area BTS mission profiles: (a) one year temperature, (b) typical one day power load and communication traffic load.

Fig. 2 shows the specific mission profiles, which are based on the typical one-day power load curve in the rural area extracted from [3] and one-year temperature data obtained in Phoenix, Arizona. The power load curve reflects the consumption of the communication traffic load, i.e., heavy load in daytime and light load in late night. Besides, according to the load curve, it can be seen that two 850 W PSUs within a 1 U power chassis [cf., Fig. 1] are enough for redundant operations in the rural area BTS.

B. Bridgeless and Conventional Boost PFC

In the previous work [2], the modified input-parallel output-series bridgeless (IPOS for short) boost, the input-parallel input-series bridgeless (IPOP) boost, and the conventional boost PFC converters IPOS boost have been designed under the same criteria and compared in terms of cost, volume,

TABLE I. Design Specifications and Selected Components

Descriptions	Parameters	Components	Parameters/Part no./Quantities
Switching frequency f_S	65 kHz	Inductors L (WF $\in 25\% \sim 40\%$)	IPOS: 254 μH, 0077094A7 ×1
Line frequency cycle f_L	60 Hz		Conv.: 508 μH, 0077730A7 ×1
RMS input voltage V_{in}	110 Vac (90∼135 Vac)	Switches + Heatsinks ($T_{cal,S} \in 100 \pm 2$°C)	IPOS: IPW65R045C7 + SW25-2G (11.4°C/W) ×2
Output voltage V_o	400 V		Conv.: IPW65R045C7 + PA-T21-38E (3.1°C/W) ×1
Output power P_o	850 W	Output capacitors C_X ($T_{cal,C} \in 95 \pm 5$ °C)	IPOS: LGG2E152MELB50 (250 V / 1500 μF) ×2
Output voltage ripple $V_{o,rip}$	$\leq$ 10 V @ 850 W		Conv.: LGG2W391MELB40 (450 V / 390 μF) ×2
RMS input current I_{in}	$\leq$10 A @ 850 W with 90 Vac	Diodes + Heatsinks ($T_{cal,D} \in 100 \pm 2$ °C)	IPOS: IDH06G65C5 + SW38-2G (10.2°C/W) ×2
Ambient temperature T_a	-20 °C to 65 °C (T_{am})		Conv.: IDH06G65C5 + SW38-2G (10.2°C/W)×1
Hold-up time t_{hold}	10 ms @ $V_{o,min}$ = 320 V	Rectifier diodes + Heatsinks ($T_{cal,DR}$* $\in 135 \pm 2$°C)	IPOS: BU2506 + YB32-4G (6.8°C/W) ×1
			Conv.: PB4006 + PA-T21-38E (3.1°C/W) ×1

* Note: $T_{cal,DR}$ is set to "135 ± 2 °C" since rectifier diodes (represented by D_R) has higher thermal stress ability than the diodes and MOSFETs.

and efficiency. The IPOS boost has the highest efficiency and the conventional boost has the lowest cost, which are the reasons why these two converters are chosen for the reliability comparison in this paper. Fig. 3 shows the targeted topologies for the reliability analysis and comparison.

Fig. 4 presents the IPOS boost operation modes in the positive half-line cycle. Due to the similarity, the operation modes in the negative half-line cycle is not given, which can be referred to in [2]. Based on the operation modes, the voltage gain of the IPOS boost is

$$\frac{V_o}{v_{in}} = \frac{2}{1 - d_{S1}} \tag{1}$$

where d_{S1} is the inductor charging duty cycle. Correspondingly, the voltage gain of the conventional boost is

$$\frac{V_o}{v_{in}} = \frac{1}{1 - d_1} \tag{2}$$

where d_1 is the inductor charging duty cycle of the conventional boost.

C. Same Component Sizing Criteria

Combining (1) and (2), if the conventional boost and the IPOS boost have the same voltage gain, there is d_{S1}=2d_1-1, i.e., d_{S1}<d_1. Fig. 5 shows the key component waveform of the IPOS and conventional boost PFC converters. It can be seen that the IPOS boost has the lower switch RMS current and larger output diode RMS current compared with the conventional boost. Thus, the power losses of these components are also different, which also affect the lifespan of the converters.

In order to ensure a fair comparison between the two studied converters, consistent component sizing are conducted in the converter design. Table I shows the design specifications and selected components for the prototypes. As can be seen in Table I, those key components, along with the heatsinks, satisfy the sizing criteria, e.g., calculated junction temperature $T_{cal,S} \in$ 100 ± 2 °C for switches. In fact, these critical components are selected from a component list based on the consistent design procedure detailed in [21].

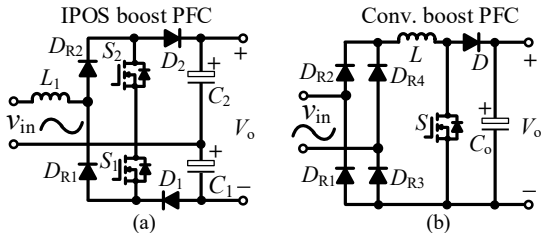

Fig. 3. Topologies for analysis: (a) IPOS boost, (b) conventional boost.

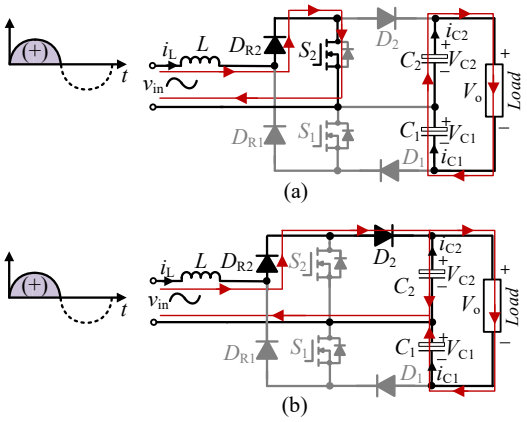

Fig. 4. IPOS boost operation modes: (a) S_2 in ON-state, (b) S_2 in OFF-state.

Based on Table I, Fig. 6 shows the corresponding prototypes with the measured efficiency curves in the experiment. The measured PF and THD_i between them are similar and can be found in [2]. Both of the prototypes use the same average current control and implemented by the TMS320F28335, located on the bottom of the board.

III. Mission Profile-Based Reliability Analysis and Results

Assumptions in this paper are summarized as follows. 1) A 1 U (=1.75 in) power chassis is assumed in the BTS and two 850 W PSUs operate in the rural area (load mission profile: 400∼450 W). 2) The load mission profile in one typical day is

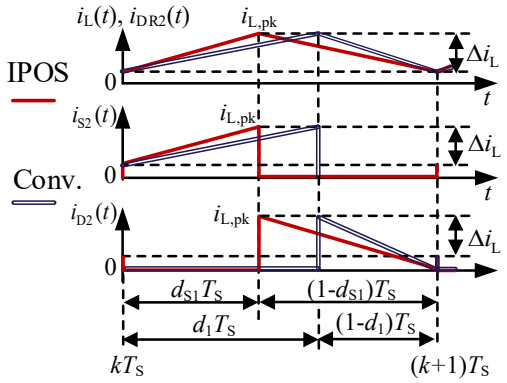

Fig. 5. IPOS and conventional boost key waveforms.

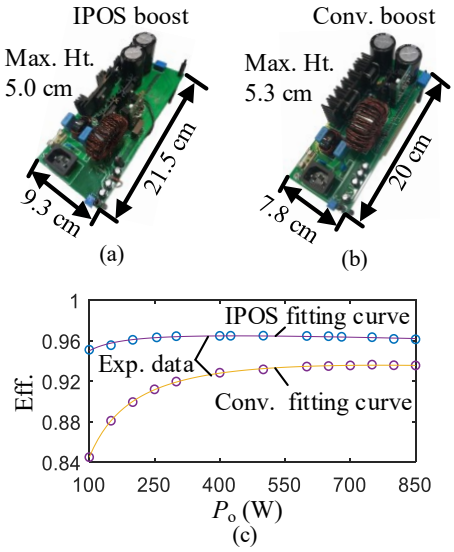

Fig. 6. Prototypes for reliability assessment and the measured efficiency curve: (a) IPOS boost prototype, (b) conventional boost prototype, (c) measured efficiency and the fitting curves Eff.(P_o) for each topology.

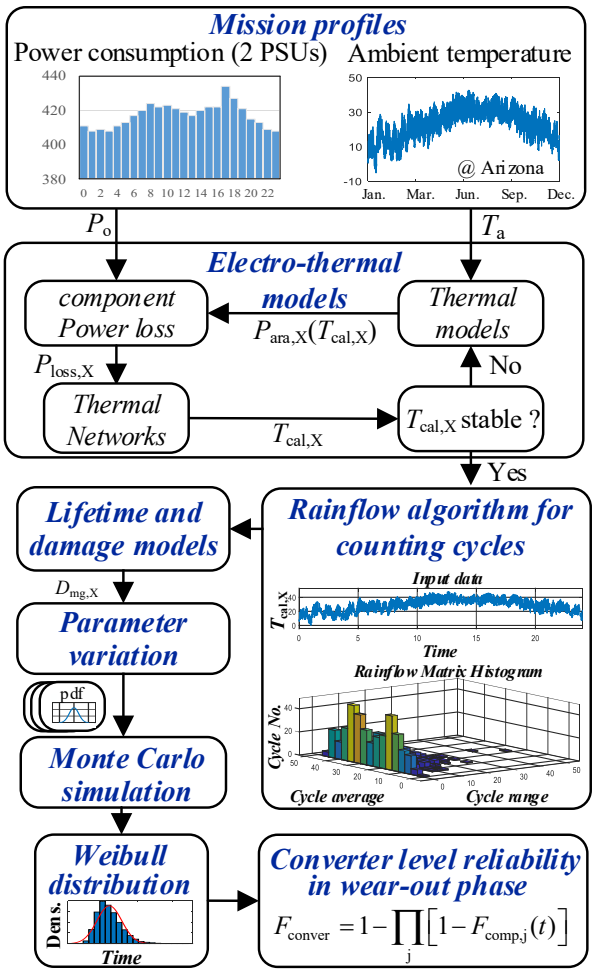

Fig. 7. Reliability analysis procedure for the converter level reliability analysis in the wear-out phase.

considered to repeat within a year. 3) The BTS is assumed in Arizona, USA, and then the one-year ambient temperature data can be used. 4) The component junction/hot-spot temperatures are assumed stable in each hour. 5) The interactive thermal impacts between components are not considered for simplicity. 6) The input voltage is considered stable in one year. 7) Capacitors and semiconductors are seen as critical components affecting the converters. 8) The wear-out phase reliability derived in this paper only considers the degradation failures described by the component lifetime models, not includes the catastrophic failures or others.

A. Reliability Analysis Procedure

Fig. 7 demonstrates the detailed reliability analysis procedure. Among the procedure, the critical parts are the mission profiles and the electro-thermal models, which makes the two converter analysis results differ from other DC-DC converters or inverters. The mission profiles mainly reflect the applications and operation condition impacts on the converter reliability. The electro-thermal models reveal the effects of the topology, component (design), and control method. As for other parts of the analysis procedure, they are conducted by following the existing algorithm, component lifetime models, statistical models, etc.

The reliability analysis procedure can be divided into two major steps, the annual damage calculation and the statistical model-related failure probability, as described below.

1) *Annual damage calculation*: Initially, combining the efficiency curves [this paper uses the fitting curve of the measured experimental efficiency in Fig. 6(c)], load mission profiles is sent to the electro-thermal model to derive the stable junction/hot-spot temperatures of the semiconductors and capacitors, and then the rainflow algorithm is adopted to collect the thermal cycle information, e.g., the mean temperature of the i^{th} identified thermal cycle. This thermal cycle information is then used in the semiconductor and capacitor lifetime models [7], [22] to estimate the annual damage. The annual damage indicates that how much the components receive the damage each year.

2) *statistical model-related failure probability*: However, the obtained annual damage results are only from a single

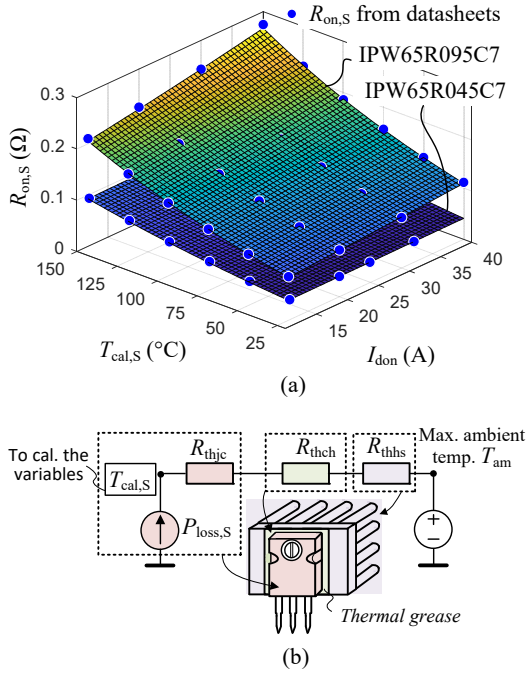

Fig. 8. Exemplified electrical and thermal network models for MOSFET key temperature derivation: (a) calculated temperature-based electrical parameters, (b) power loss-related thermal networks.

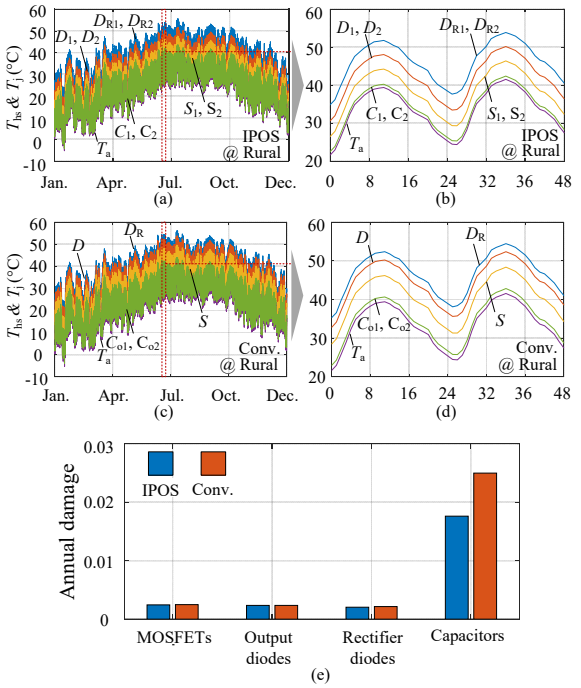

Fig. 9. Calculated junction/hot-spot temperatures of critical components over one year and the relative annual damages: (a)∼(d) key temperatures, (d) annual damage.

sample. In reality, many variations can cause annual damage differences between components. Thus, the various statistical models of main parameters are used to present these variations and the Monte Carlo simulation is conducted to show these possible results with a large group of samples.

B. Annual Damage Calculation

The electro-thermal loop is dependent on the specific component properties. Fig. 8 shows the exemplified electrical and thermal network models of MOSFETs used in this paper. It includes two major parts, $T_{\mathrm{cal,S}}$ based on-state resistance curve fitting model for the accurate power loss estimation and the power loss-related thermal network for the calculation of junction temperature $T_{\mathrm{cal,S}}$. Through the built models exemplified in Fig. 8, the calculated junction/hot-spot temperatures of the key components can be derived.

Because the calculated junction/hot-spot temperatures over one year are difficult to be used directly in the existing component lifetime models, the rainflow algorithm is employed to identify the thermal cycles and collect the thermal cycle information, e.g., thermal cycle number n_{i} for the ith identified thermal cycle, temperature variation $\Delta T_{\mathrm{cal,X,i}}$ for the ith identified thermal cycle. Meanwhile, according to [22], a MOSFET cycle-to-failure model with critical parameters m and α fitted by experiment data is used as

$$N_{\mathrm{f,i}} = \alpha \cdot (\Delta T_{\mathrm{cal,S,i}})^{-m} \tag{3}$$

in which $N_{\mathrm{f,i}}$ is the cycle-to-failure under the ith thermal cycle condition. Then, a widely-used linear accumulation of damage model [22]–[24] is adopted to estimate the accumulative damage $D_{\mathrm{mg,semi}}$ in one year, which is expressed by the thermal cycle number n_{i} and $N_{\mathrm{f,i}}$ as

$$D_{\mathrm{mg,semi}} = \sum_{\mathrm{i}} (n_{\mathrm{i}}/N_{\mathrm{f,i}}) \tag{4}$$

As for the Al-Cap, a popular lifetime evaluation model is used [7], as

$$L_{\mathrm{C,i}} = L_{\mathrm{C0}} \cdot 2^{\frac{T_0 - T_{\mathrm{hs,i}}}{10}} (V_{\mathrm{C}}/V_0)^{-n_0} \tag{5}$$

where L_{C0} is the lifetime under the temperature T_0 and rated voltage V_0, $L_{\mathrm{C,i}}$ the estimated capacitor lifetime of the ith cycle, $T_{\mathrm{hs,i}}$ the mean hot-spot temperature identified in the ith cycle, V_{C} the applied voltage, and n_0 the voltage stress exponent. Here n_0 is equal to 3 by referring to [7]. And then the accumulative damage $D_{\mathrm{mg,cap}}$ in one year is

$$D_{\mathrm{mg,cap}} = \sum_{\mathrm{i}} (\Delta L_{\mathrm{i}}/L_{\mathrm{C,i}}) \tag{6}$$

where ΔL_{i} is the ith identified thermal cycle range.

Fig. 9 shows the critical component temperatures of the IPOS and conventional boost over one year and the corresponding component annual damage. It can be seen that for the studied PFC converters, the Al-Caps are the weakest part in terms of the reliability performance.

C. Probability Failure Probability

In reality, there are always slight differences between individuals, test results, measurements, etc. These differences [18], [19], [25] may be caused by the different material microstructures, transportation effects, cosmic radiations, human-

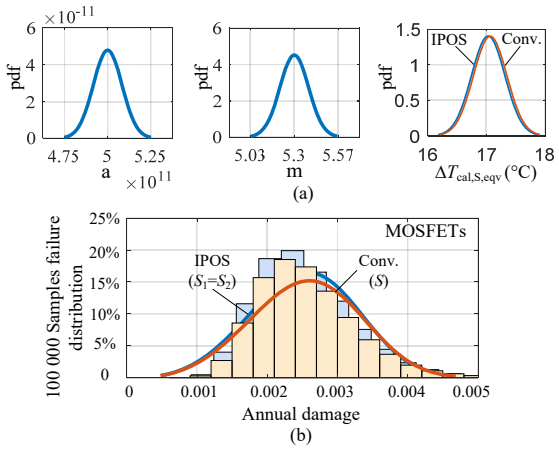

Fig. 10. Reliability analysis of MOSFETs in the IPOS and conventional boost: (a) parameter probability density functions with 5% variations, (b) histograms of 100 000 samples' wear-out failure distributions.

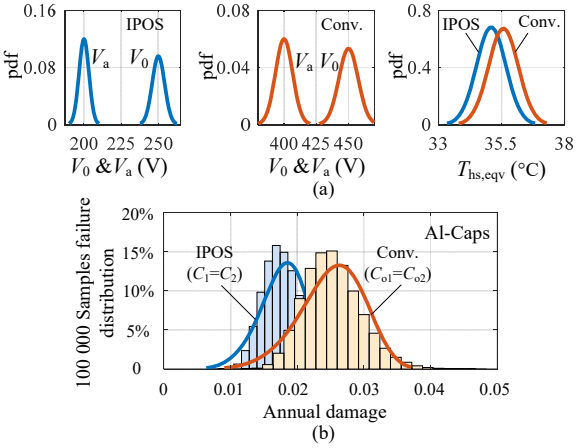

Fig. 11. Reliability analysis of Al-Caps in the IPOS and conventional boost: (a) parameter probability density functions with 5% variations (pdfs of L_0, n_0, and T_0 are not shown here for brevity.), (b) histograms of 100 000 samples' wear-out failure distributions.

related behavior, etc. Thus, in order to describe these variations, the statistical models are introduced in the reliability analysis procedure.

Specifically, the measurements, constants in equations, and test results usually follow the Normal/Gaussian distributions, while, the system level times-to-failure determined by the weakest component, e.g., semiconductor failure caused by the dielectric degradation, are well described by the Weibull distribution [25]. Thus, each parameter in lifetime models (3) and (5) can be described by the probability density function (pdf) of the Normal distribution. And the annual damage of the components can be fitted by the pdf of the Weibull distribution.

$D_{\mathrm{mg,semi}}$ and $D_{\mathrm{mg,cap}}$ derived in the last part can be seen as the results determined by the equivalent static values and then the statistical models can be introduced by setting certain variations of the equivalent static values. Just as a resistant power loss caused by the dynamic flowing current can be equivalent to a square of RMS current times the resistance, $D_{\mathrm{mg,semi}}$ and $D_{\mathrm{mg,cap}}$ can also be seen as the results determined by the equivalent static values, as

$$D_{\mathrm{mg,semi}} = \frac{365}{N_{\mathrm{f,eqv}}} = \frac{365}{\alpha \cdot (\Delta T_{\mathrm{cal,X,eqv}})^{-m}} \tag{7}$$

$$D_{\mathrm{mg,cap}} = \frac{24 \times 365}{L_{\mathrm{C,eqv}}} = \frac{8760}{L_{\mathrm{C0}} \cdot 2^{\frac{T_0 - T_{\mathrm{hs,eqv}}}{10}} (V_{\mathrm{C}}/V_0)^{-n_2}} \tag{8}$$

where 365 days are considered as 365 cycles in one year with the corresponding $\Delta T_{\mathrm{cal,X,eqv}}$ to fit the derived $D_{\mathrm{mg,semi}}$ and 8760 hours in one year are used with $T_{\mathrm{hs,eqv}}$ to fit $D_{\mathrm{mg,cap}}$. By (7) and (8), $\Delta T_{\mathrm{cal,X,eqv}}$ and $T_{\mathrm{hs,eqv}}$ can be derived. Then, given the 5% variations of each parameter, their pdfs can be obtained as shown in Figs. 10(a) and 11(a).

Monte Carlo simulation uses the random sampling data to reveal a deterministic answer for a question full of uncertainties and boundaries, e.g., the lifetime of one product, accessibility of one scheduled plan, risk of investment failure. Here, Monte Carlo simulation is conducted to explore the possible failures based on the different input parameters from

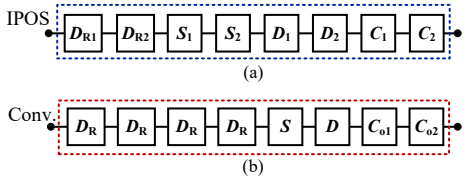

Fig. 12. Considered reliability block diagram (RBD) for converter-level reliability calculations: (a) IPOS boost and (b) conventional boost.

100 000 samples. Then, the obtained data is fitted by Weibull distribution [18]–[20], which is

$$f_{\mathrm{comp,j}}(t) = \frac{\beta}{\eta}\left(\frac{t}{\eta}\right)^{\beta-1} e^{-\left(\frac{t}{\eta}\right)^{\beta}}, F_{\mathrm{comp,j}}(t) = 1 - e^{-\left(\frac{t}{\eta}\right)^{\beta}} \tag{9}$$

where β is the scale parameter, η the shape parameter, and $F_{\mathrm{comp,j}}$ the corresponding cumulative distribution function (cdf) of the component j. Afterward, the converter-level reliability block diagram (RBD) of the IPOS and conventional boost are used, as shown in Fig. 12. Provided that the failure of one critical component can make the whole system fail, the converter-level failure function is expressed as

$$F_{\mathrm{conver}} = 1 - \prod_{\mathrm{j}} [1 - F_{\mathrm{comp,j}}(t)]. \tag{10}$$

Fig. 13 shows the accumulated failure probability curves of the IPOS and conventional boost PFC converters and the corresponding components. Under the investigated mission profiles, the estimated accumulated failure of the IPOS boost within 20 years of operation is $0.27\,\%$, much lower than that of the conventional boost, which is $2.06\,\%$. Even though the estimated payback period of using the IPOS boost topology instead of the conventional boost is 3.9 years in the rural area [2], given the relatively high maintenance cost in the rural area, the IPOS boost topology with the much lower failure percentage is still an attractive solution.

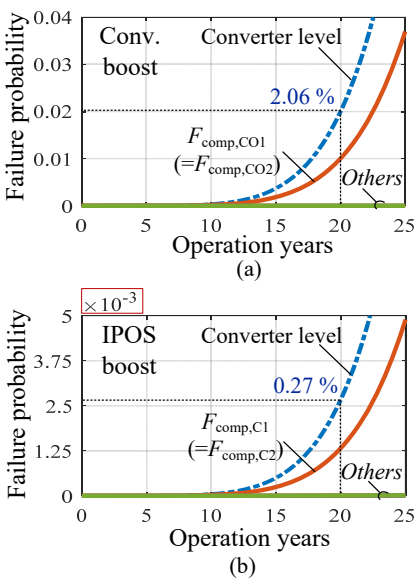

Fig. 13. Estimated accumulative wear-out failure probability curves of the compared converters: (a) conventional boost, (b) IPOS boost. Note that here "Others" represent the semiconductors, including MOSFETs, output diodes, and the input rectifier diodes.

IV. Conclusion

Based on the telecom TBS mission profiles in a rural area and by following the reliability analysis procedure, this digest estimates the accumulative wear-out failure probability of the bridgeless IPOS boost and the conventional boost PFC converters, both of which are designed under the same criteria. The analysis results indicate that given 20 years targeted lifetime, the IPOS boost has an accumulated failure $0.27\,\%$ due to the wear-out failure of semiconductors and capacitors, much lower than that of the conventional boost ($2.06\,\%$). Given the relatively high maintenance cost in the rural area, the IPOS bridgeless boost topology is a good candidate for the TBS applications in the rural area.

References

[1] L. Huber, Y. Jang, and M. M. Jovanović, "Performance evaluation of bridgeless PFC boost rectifiers," *IEEE Trans. Power Electron.*, vol. 23, no. 3, pp. 1381–1390, May. 2008.

[2] Z. Chen, P. Davari, and H. Wang, "Single-phase bridgeless PFC topology derivation and performance benchmarking," *IEEE Trans. Power Electron.*, vol. 35, no. 9, pp. 9238–9250, Sep. 2020.

[3] B. Huang, G. Torrico, X. Ma, and Y. Liang, "High efficiency telecom rectifier designed for wireless communication networks," in *Proc. Int. Telecom. Energy Conf.*, pp. 1–6, 2011.

[4] F. Musavi, W. Eberle, and W. G. Dunford, "A high-performance single-phase bridgeless interleaved PFC converter for plug-in hybrid electric vehicle battery chargers," *IEEE Trans. Ind. Appl.*, vol. 47, no. 4, pp. 1833–1843, Jul. 2011.

[5] S. Allemann, J. Biela, and M. Held, "Reliability comparison of a dual boost and a triangular current mode resonant-transition PFC converter topology," in *Proc., Int. Conf. Integ. Power Electron. Syst.*, pp. 1–5, 2012.

[6] H. Ma, J. Lai, C. Zheng, and P. Sun, "A high-efficiency quasi-single-stage bridgeless electrolytic capacitor-free high-power AC-DC driver for supplying multiple LED strings in parallel," *IEEE Trans. Power Electron.*, vol. 31, no. 8, pp. 5825–5836, Aug. 2016.

[7] H. Wang and F. Blaabjerg, "Reliability of capacitors for DC-link applications in power electronic converters - an overview," *IEEE Trans. Ind. Appl.*, vol. 50, no. 5, pp. 3569–3578, Sep./Oct. 2014.

[8] A. Lahyani, P. Venet, G. Grellet, and P. J. Viverge, "Failure prediction of electrolytic capacitors during operation of a switchmode power supply," *IEEE Trans. Power Electron.*, vol. 13, no. 6, pp. 1199–1207, Nov. 1998.

[9] K. Abdennadher, P. Venet, G. Rojat, J. Rétif, and C. Rosset, "A real-time predictive-maintenance system of aluminum electrolytic capacitors used in uninterrupted power supplies," *IEEE Trans. Ind. Appl.*, vol. 46, no. 4, pp. 1644–1652, Jul./Aug. 2010.

[10] B. Sun, X. Fan, C. Qian, and G. Zhang, "PoF-simulation-assisted reliability prediction for electrolytic capacitor in LED drivers," *IEEE Trans. Ind. Electron.*, vol. 63, no. 11, pp. 6726–6735, Nov. 2016.

[11] A. H. Ranjbar, B. Abdi, G. B. Gharehpetian, and B. Fahimi, "Reliability assessment of single-stage/two-stage PFC converters," in *Proc., Compat. Power Electron.*, pp. 253–257, 2009.

[12] B. Abdi, A. H. Ranjbar, J. Milimonfared, and G. B. Gharehpetian, "Reliability comparison of boost PFC converter in DCM and CCM operating modes," in *Proc., Int. Sym. Power Electron., Elec. Drives, Auto. Motion*, pp. 939–943, 2008.

[13] H. Valipour, M. Fotuhi Firouzabad, G. Rezazadeh, and M. R. Zolghadri, "Reliability comparison of two industrial AC/DC converters with resonant and non-resonant topologies," in *Proc., Power Electron. Drive Syst. Tech. Conf.*, pp. 430–435, 2015.

[14] Y. Song and B. Wang, "Survey on reliability of power electronic systems," *IEEE Trans. Power Electron.*, vol. 28, no. 1, pp. 591–604, Jan. 2013.

[15] J. W. Harms, "Revision of MIL-HDBK-217, reliability prediction of electronic equipment," in *Proc., Ann. Rel. Maintainability Sym.*, pp. 1–3, 2010.

[16] G. A. Klutke, P. C. Kiessler, and M. A. Wortman, "A critical look at the bathtub curve," *IEEE Trans. Rel.*, vol. 52, no. 1, pp. 125–129, Mar. 2003.

[17] H. Wang, M. Liserre, F. Blaabjerg, P. de Place Rimmen, J. B. Jacobsen, T. Kvisgaard, and J. Landkildehus, "Transitioning to physics-of-failure as a reliability driver in power electronics," *IEEE J. Emerg. Sel. Topics in Power Electron.*, vol. 2, no. 1, pp. 97–114, Mar. 2014.

[18] D. Zhou, H. Wang, and F. Blaabjerg, "Mission profile based system-level reliability analysis of DC/DC converters for a backup power application," *IEEE Trans. Power Electron.*, vol. 33, no. 9, pp. 8030–8039, Sep. 2018.

[19] Y. Shen, A. Chub, H. Wang, D. Vinnikov, E. Liivik, and F. Blaabjerg, "Wear-out failure analysis of an impedance-source PV microinverter based on system-level electro-thermal modeling," *IEEE Trans. Ind. Electron.*, vol. 66, no. 5, pp. 3914–3927, May. 2019.

[20] Y. Zhang, H. Wang, Z. Wang, F. Blaabjerg, and M. Saeedifard, "Mission profile-based system-level reliability prediction method for modular multilevel converters," *IEEE Trans. Power Electron.*, vol. 35, no. 7, pp. 6916–6930, Jul. 2020.

[21] Z. Chen, B. Liu, Y. Yang, P. Davari, and H. Wang, "Bridgeless pfc topology simplification and design for performance benchmarking," *IEEE Trans. Power Electron.*, vol. 36, no. 5, pp. 5398–5414, May. 2021.

[22] A. Testa, S. De Caro, and S. Russo, "A reliability model for power MOSFETs working in avalanche mode based on an experimental temperature distribution analysis," *IEEE Trans. Power Electron.*, vol. 27, no. 6, pp. 3093–3100, Jun. 2012.

[23] M. A. Miner, "Cumulative damage in fatigue," *Trans. ASME. J. Appl. Mech.*, vol. 12, pp. A–159–A–164, Sep. 1945.

[24] S. Russo, A. Testa, S. De Caro, T. Scimone, S. Panarello, S. Patanè, G. Scelba, and G. Scarcella, "Reliability assessment of power MOSFETs working in avalanche mode based on a thermal strain direct measurement approach," *IEEE Trans. Ind. Appl.*, vol. 52, no. 2, pp. 1688–1697, Mar. 2016.

[25] J. W. McPherson, *Reliability Physics and Engineering Time-To-Failure Modeling*, 1st ed. Switzerland: Springer Int., 2013.